THE PENNSYLVANIA STATE UNIVERSITY
SCHREYER HONORS COLLEGE

DEPARTMENT OF ASTRONOMY AND ASTROPHYSICS

DETECTING TYPE II-P SUPERNOVA PRECURSOR EMISSION VIA MACHINE LEARNING

ANNA TARTAGLIA
SPRING 2024

A thesis
submitted in partial fulfillment
of the requirements
for baccalaureate degrees
in Astronomy & Astrophysics and Physics
with honors in Astronomy & Astrophysics

Reviewed and approved* by the following:

Dr. Donald P. Schneider
Distinguished Professor of Astronomy and Astrophysics
Thesis Supervisor

Dr. Cindy Yuexing Gulis
Associate Professor of Astronomy and Astrophysics
Honors Adviser

*Signatures are on file in the Schreyer Honors College.

Abstract

The final years of Red Supergiant (RSG) stars present a challenging observational window. However, insights gleaned from photometric and spectroscopic measurements of Type II-P supernovae reveal evidence of eruptive mass loss events in these stars, which precede supernova shock breakout (SBO) by months to years. With limited observation and modeling capabilities within this critical timeframe, the driving mechanisms behind these eruptions, their manifestations, and subsequent impacts on stellar evolution remain elusive. In this paper, we construct and train a Convolutional Neural Network to detect precursor eruptions within light curves. The network is designed in preparation for the forthcoming Vera C. Rubin Legacy Survey of Space and Time (LSST), a 10-year Southern sky survey anticipated to revolutionize transient observations. We develop models of eruptions and wield them to simulate realistic light curves in the depth and cadence of LSST for network training. Our study estimates a predicted detection rate of $\sim 11 - 50$ precursor events per year, depending on different parameter distributions. The network exhibits strong performance for nearby events, with reliable detections achievable up to $z \lesssim 0.03$. In cases where precursors remain undetected, our network can still offer significant insights by delineating the limits of potential precursor events. These insights will contribute to a deeper understanding of the nuanced processes underlying stellar evolution and transient phenomena.

Table of Contents

List of Figures

Acknowledgements

I would first like to thank Dr. Ashley Villar, who has provided immense support and guidance throughout this project and my undergraduate career as a whole. Her support as an advisor and mentor has continued to inspire me to reach my full potential. Thank you to Dr. Donald Schneider, whose classes invigorated my passion for the field and whose support has been invaluable in shaping my journey as a scientist.

Thank you to my parents—you were the first ones to support my aspirations. You took me to the planetariums and movies and mountains, watched the documentaries with me, showed me the constellations, and pointed me towards the North Star. Your continued belief in me has been pivotal to my success.

To Ande, who continues to ground me. We have been in harmony ever since you sat next to me in Language Arts—literally.

To Jade—I would not be who or where I am without you. We will always be laughing 'til our ribs get tough!

To Shana, who has been here with me every step of the way since first year E&M.

And, finally I would like to thank Meysoon. My best friend, other half, life coach, hive member, wizard, tribute, partner, no cash, no credit—you have always believed in me. This is just the first of many acknowledgements, all on the path to our final form: co-authorship. Here's to a lifetime of "liking to go out but loving a night in."

Chapter 1

Introduction

1.1 Late-Stage SNe II-P Precursor Mass Loss

Hydrogen-rich Type II-P supernovae (SNe II-P) are the most common type of core-collapse supernovae, characterized by a "plateau" feature in their light curves. Their progenitor stars are primarily red supergiants (RSGs; although other types such as blue supergiants and yellow supergiants can explode as SNe II-P [3, 4]). The physical conditions preceding these SNe (especially within the final years of stellar lifespan) are difficult to observe. They are, additionally, extremely difficult to model, as the time frames are very short in comparison to the large-time steps of full-lifetime stellar evolution codes. Circumstellar material (CSM), however, can allow insight into the progenitor star mechanisms and environments [5].

Multi-band observations of red supergiants (RSGs) reveal a surplus of circumstellar dust surrounding the stars. Specifically, emission from these stars in the infrared (IR) band detected via photometry and spectroscopy indicates this surplus, as dust re-emits photons in the IR. High, variable levels of extinction measured in RSG observations are also attributed to dust (the variability suggests this dust is produced irregularly) [6]. The presence of this CSM is evidence for significant mass loss during the RSG phase of evolution, when surface gravity is low [7].

The mechanisms that drive RSG mass loss are uncertain. The temperature of these cooler stars ($\sim 3500 - 4500$ K) is not sufficient for line-driven winds (i.e. winds generated by radiation pressure on spectral lines). Dust-driven winds may contribute to enriched CSMs [7], however, this implies a simple relation between luminosity L and $\dot{M}$; in empirical measurements of RSGs, there is significant scatter in this relation, indicating that this mechanism cannot be the only form of mass loss at play [8, 9]. There is, additionally, evidence for eruptive, episodic mass loss: spatial interferometric measurements reveal that the circumstellar dust often takes asymmetric, shell-like configurations [10, 11]. Other proposed drivers of mass loss include:

- Radial pulsations caused by partial hydrogen ionization. The pulsations could generate shocks and dust waves that boost stellar winds. Models of this phenomenon by Yoon & Cantiello (2010) find that it can potentially drive mass loss rates up to $\sim 10^{-3}\ M_\odot$ yr^{-1} [12].

- Dissipation of Alfvén waves, in which a propagating magnetic field drives ions through the stellar material and boosts winds. It is not known exactly how much this process amplifies mass loss. Hartmann & Avrett (1984) modeled Alfvén wave mass loss in Betelgeuse, assuming the mechanism drove a mass loss rate on the order of $10^{-5}\ M_\odot$ yr^{-1} [13].

- Supra-Eddington mass loss, in which the Eddington limit drops below the stellar luminosity, causing enhanced mass expulsion [7, 8]. One such model of this process found mass loss rates of $\sim 10^{-5}\ M_\odot$ yr^{-1} and calculated a minimum mass of stars undergoing it ($\sim 20 M_\odot$) which is higher than the most luminous II-P progenitors [14, 15].

Mass loss rates play a significant role in determining the evolution of the RSG [5]. As a result of the uncertainty in mechanisms, these rates can not be determined from first principles. Instead, astronomers rely on empirical observations to inform stellar evolution models and, subsequently, SN light curve models [16].

Current models of SNe II-P fail to replicate key features observed in II-P light curves; specifically, the SNe exhibit brighter, hotter peaks in emission and shorter rise times. An example of one such II-P lightcurve (SN 2016bkv) is shown in Figure 1.1. Additionally, shock breakout (SBO; when the SN shock breaks through the star) of these lightcurves can extend to the timescale of days, rather than the expected timescale of hours. These disparities indicate the presence of an unaccounted-for circumstellar medium (CSM) surrounding the progenitor at the time of SBO [17]. The CSM shell enhances SNe luminosity by transforming the kinetic energy of the ejected material into thermal energy. This, combined with the extended radius formed by the shell, explains the accelerated and bright peaks observed in the light curves. Extended SBO is attributed to the shock having to break out of an optically thick shell at a larger radius [18].

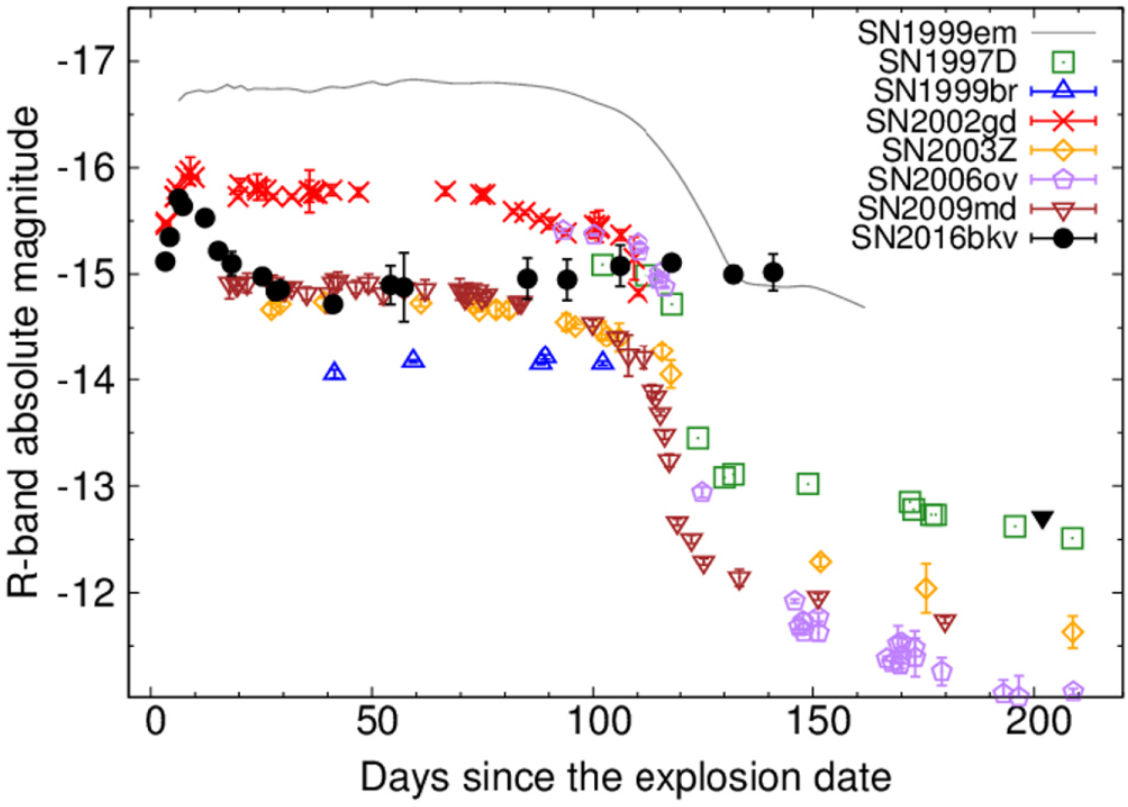

Figure 1.1: Reproduced from Nakaoka et al. (2018) [1]. The r-band light curve of SN2016bkv (black), a II-P SN which displayed a fast, bright peak within the first $\sim$ 7 days following SBO. The light curve is compared with those of other II-P SNe (1997D, 1999br, 2002gd, 2003Z, 2006ov, 2009md, and SN1999em.)

Furthermore, SNe II-P observations are accompanied by flash-spectroscopic measurements that reveal narrow hydrogen emission lines [19]. These lines only appear within tens of hours to days following SBO and are attributed to shockwave interaction with the circumstellar shell, in which the material comprising the CSM is photoionized by the SN light [20]. Their features (e.g. strength, width, and duration) illuminate characteristic features of the CSM; notably, the short-lived presence of the emission lines indicates a circumstellar shell that is dense and compact, and consequently likely arises from eruptive mass loss events within the final months to year of the progenitor's life [21, 22]. Mass loss rates $\dot{M} \sim 10^{-4} - 10^{-2}\ M_{\odot}\ \mathrm{yr}^{-1}$ are inferred (via radiative transfer stellar models) from these spectra [19].

The most cited physical explanation for the described precursors attributes them to late-stage nuclear burning of oxygen, neon, and silicon in the stellar core. In this model, introduced by Quataert & Shiode (2012; 2014) [23, 24], convection in the core generates gravity waves that transfer energy into the stellar envelope, ultimately resulting in an eruption and mass ejection into the surrounding stellar environment. Models of this hypothesized phenomenon by Morozova et al. (2020) [17] and Wu & Fuller (2021) [25] find energy injections of 10^{46} to 10^{47} ergs into the stellar core produce eruptive events and subsequent SN interactions that can explain observed LC features. These eruptions are capable of ejecting up to a solar mass of material into the CSM [26] and would occur within the final years preceding the SN (or, in the case of eruptions generated by silicon burning, the final weeks) [27].

1.2 Previous Precursor Detections

Precursor events have been observed in Type IIn SNe, accompanied by evidence of shockwave CSM-interaction in spectra [28]. Some notable outbursts include those which preceded SN 2009ip [29, 30], 2010mc [31], 2011ht [32], iPTF13z [33], LSQ13zm [34], 2016bdu [35], 2018cnf [36]. However, only one unambiguous precursor detection has been made in a Type II-P SN; optical observations of pre-SN emission paired with flash spectroscopy evidence of CSM presence indicate an eruptive event preceded SN 2020tlf [19]. More observational data of pre-SN eruptions can potentially serve as a probe to demystify large uncertainties regarding their nature (e.g. timescales, occurrence rates, progenitor populations, driving mechanisms, and more).

1.3 Vera C. Rubin Legacy Survey of Space and Time

The Legacy Survey of Space and Time (LSST) [37] is an upcoming 10-year, deep-field survey of the southern sky by Vera C. Rubin telescope in northern Chile. The survey, anticipated to begin operations in 2025, will collect observations in the $ugrizy$ bands over approximately 18,000 deg^2

of the sky every 3 days [38]. One of LSST's primary science goals is transient discovery. The survey's deep, wide, and temporally compact coverage will dramatically increase current catalogs of transients ($\sim$10 million alerts are expected every night) and unveil unprecedented volumes of new objects (including previously unseen types) [39].

We expect precursor observations to increase with these new catalogs. The survey's 3-day cadence allows for the detection of short-lived events such as the expected eruptions. In anticipation of LSST, now is the optimal time to construct detection pipelines capable of sifting through the mass light curve data outputs to discover precursors and enrich current scientific understandings of their nature.

1.4 A Precursor Detection Pipeline

In this paper, we construct an algorithm utilizing machine learning to detect pre-SN emission in LSST light curve data. In Chapter 2, we describe our adiabatic model of precursor eruptions and subsequent generation of synthetic light curves. Chapter 3 discusses the design of our convolutional neural network, which classifies whether given light curves contain precursors. In Chapter 4, we evaluate the detection capacity of our algorithm. We conclude in Chapter 5

Chapter 2

Producing Neural Network Training Data

2.1 Adiabatic Eruption Model

To simulate realistic light curves, we first develop a model of the pre-SN bursts. In our model, the eruption produces a CSM shell, expanding from the progenitor star radius, R_0, at a constant velocity v, such that

$$R = R_0 + vt \tag{2.1}$$

where t is the time since the burst onset. The shell radiates as a blackbody spectral energy distribution (SED); its luminosity adheres to transient adiabatic expansion (i.e., without a heating source):

$$L = L_0 e^{\frac{-t}{t_0}} \tag{2.2}$$

[40, 41]. In this equation, L_0 denotes the initial injected luminosity of the burst. The eruption diffusion time, t_0, is calculated as

$$t_0 = \frac{\kappa M}{\beta c R_0} \tag{2.3}$$

where c refers to the speed of light, the opacity κ is set to H-rich opacity .3 cm^2/g, β is a constant determined by the density profile [42] which we set to 13.7. The ejecta mass, M, may vary (free parameter constraints are discussed below).

The shell inflates until the black body temperature falls to the hydrogen-recombination temperature (3000 K). After reaching this point, it begins contracting to maintain a constant temperature. The model spans the duration of a year from burst onset.

Three free parameters may be varied to produce diverse sets of models: ejecta mass M, ejecta velocity v, and injected burst luminosity L_0. We range ejecta mass values between $.1 - 1 M_\odot$, ejecta velocity between $50 - 1000$ km/s, and injected burst luminosity between $10^5 - 10^7 L_\odot$. These ranges reflect those predicted in wave-driven precursor eruption simulations by Fuller (2017) [26] and Matsumoto & Metzger (2022) [27]. Figures 2.1 and 2.2 display the model diversity over parameter spaces.

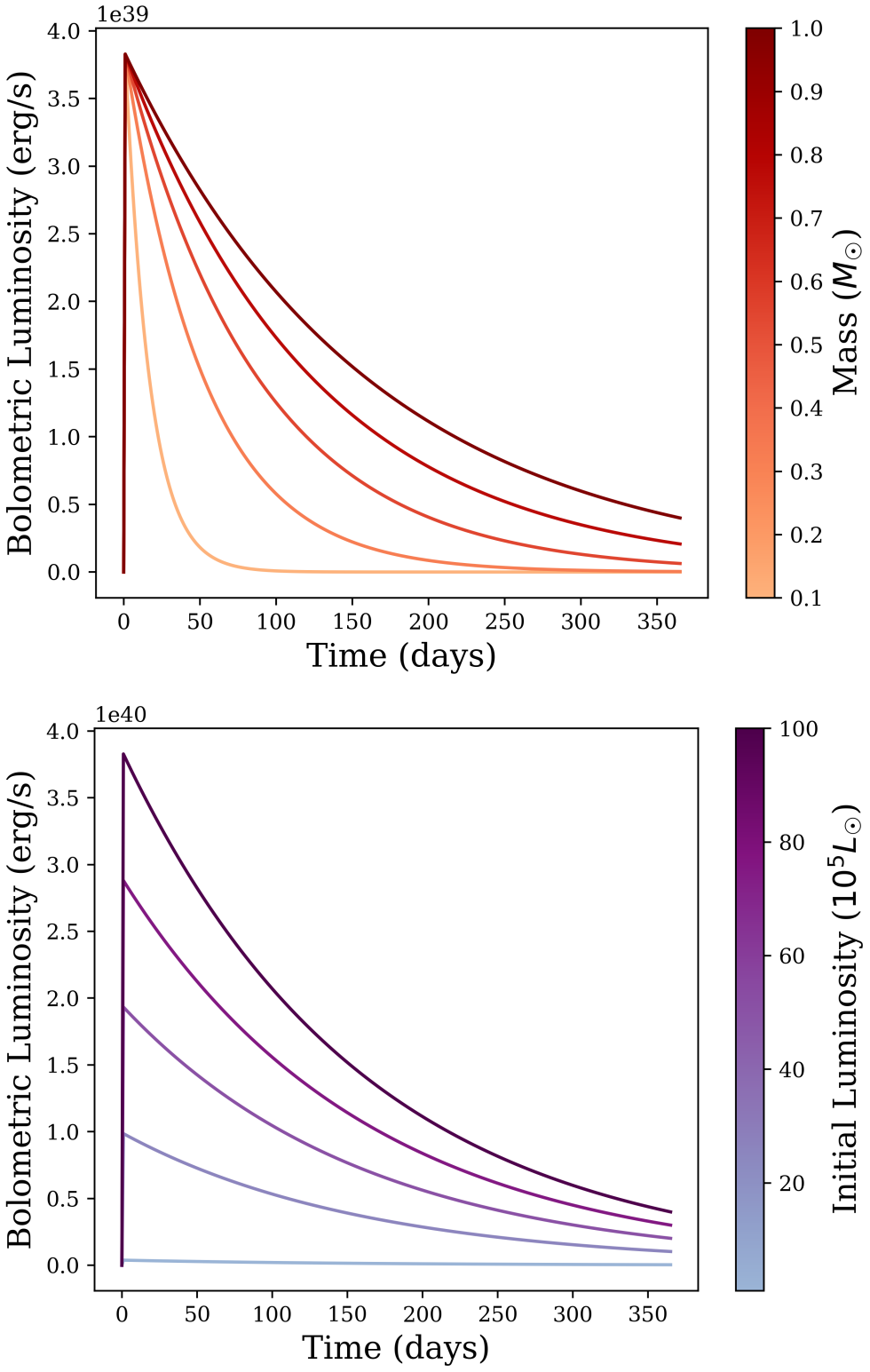

Figure 2.1: Bolometric light curves of the model eruption plotted over the ranges of free parameters M and L_0. In the top graph, M ranges while L_0 remains constant at $10^6 L_\odot$ and v is held constant at 50 km/s. In the bottom graph, we range L_0 and hold $M = 1 M_\odot$ and $v = 50$ km/s constant.

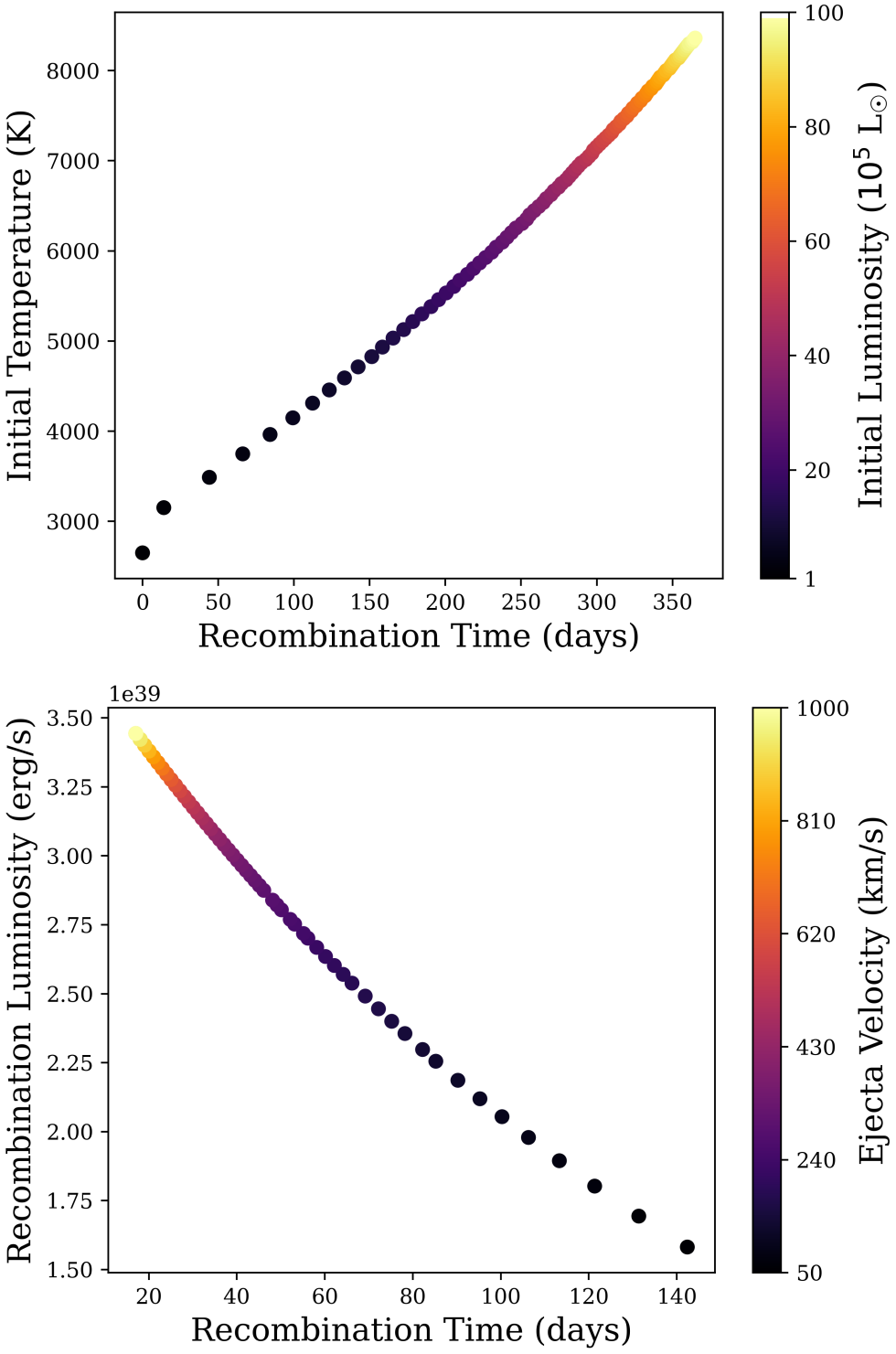

Figure 2.2: Model diversity over burst luminosity L_0 (top) and velocity v (bottom). These plots present the time (in days after eruption) of hydrogen recombination (when $T = 3000$), the initial temperature T_0, and the luminosity at the time of recombination over L_0 and v parameter ranges. In the upper graph, $v = 50$ km/s and $M = 1M_\odot$. In the lower, $L_0 = 10^6 L_\odot$ and $M = 1M_\odot$.

2.2 LSST Light Curve Simulation

We use the simulation software `OpSim` (Operations Simulator) [43] to generate light curve sets of our modeled eruptions for use in neural network training. `OpSim`'s high-precision model reproduces internal mechanical conditions and constraints of the LSST telescope system along with the observing patterns and scope. It simulates weather patterns and environmental factors that affect time-series data, producing realistic light curve data of the synthetic observation in the survey cadence.

Each light curve injects a model at a random sky location (within the LSST field), modified Julian date (MJD) time, and redshift. Each injected model is also randomized in parameter space within the ranges denoted in Section 2.1. LSST light curves contain AB magnitude data in the $ugrizy$ bands. Our training data set includes light curves in which no eruption is injected, to allow the the network to learn how to classify precursor presence.

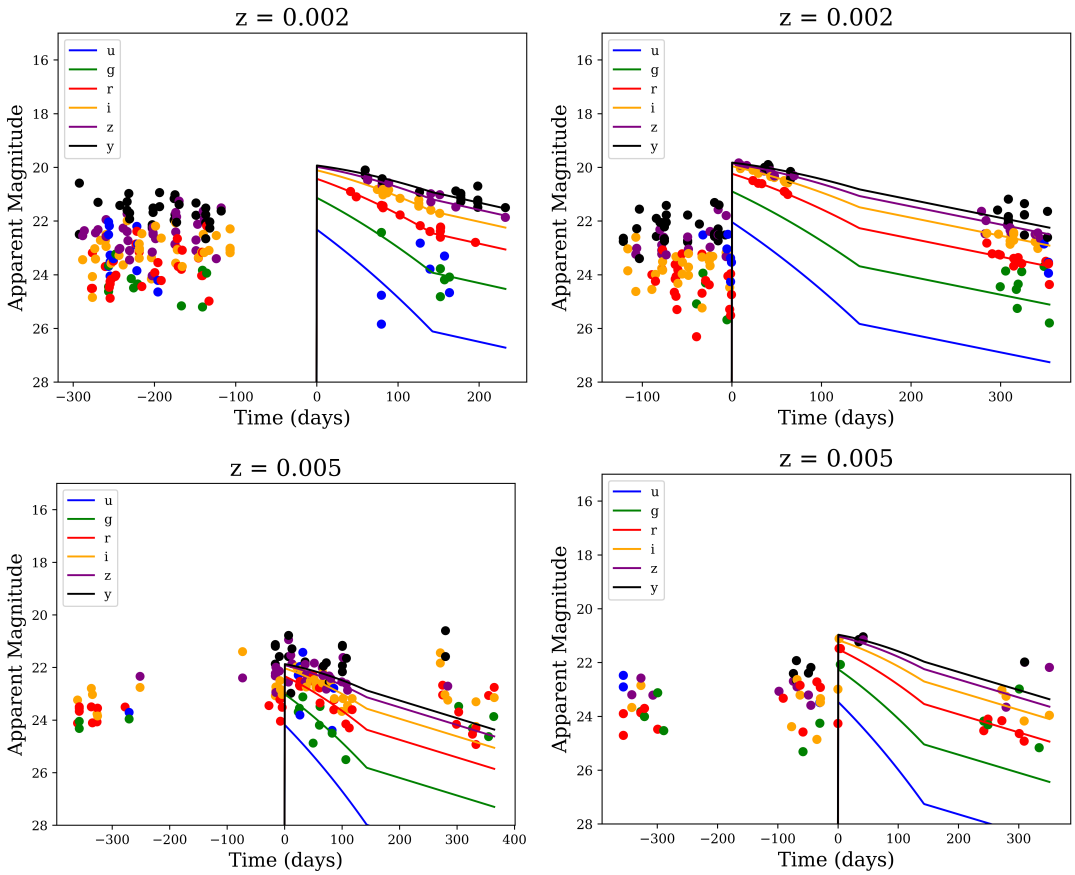

Figure 2.3: Example simulated light curves of injected $1M_{\odot}$ eruption with a 50 km/s ejecta velocity and $10^6 L_{\odot}$ initial luminosity at redshifts $z = .002$ (top row) and $z = .005$ (bottom row). Light curves (scatter) are plotted over the underlying model (solid line) in the $ugrizy$ bands. The time $t = 0$ refers to the time of eruption.

Chapter 3

Classification Neural Network

3.1 Convolutional Neural Network

In this chapter, we discuss our classification neural network (NN), which is used to detect precursor eruptions in LSST light curves. Initially, our efforts focused on constructing a Recurrent Neural Network (RNN) for this task, a popular choice for handling time-series data due to its intrinsic memory mechanisms [44]. RNNs are adept at processing sequential data, such as speech or handwriting recognition, by incorporating information from previous inputs at each sequential data point. However, our attempts with the RNN proved unsuccessful in effectively classifying the light curves. The dimness of our eruptions and general variability of the light curves may have contributed to RNN limitations, along with the large gaps featured in LSST data.

Instead, we develop a convolutional neural network (CNN) [45] capable of taking in light curve data and classifying the presence of a pre-SN eruption. This type of network contains convolutional layers, which perform convolutions over two-dimensional data. It is often used for images, as the convolutional layers are well suited for pattern recognition tasks. Convolution takes a tensor of numbers (called a *kernel*) and slides it along the input data tensor, computing the element-wise product of the overlapping section at each ”slide” location. Refer to Figure 3.1 for a depiction of this mapping. These convolutions are capable of distinguishing features in the data, such as edges or shapes in an image, depending on the specific kernel used. The process of training the CNN, then, includes optimizing the kernels used in these layers according to the given problem. After convolution, the layer passes the data through a non-linear *activation function*. The non-linearity is essential for the network to learn, as it allows it to discern more complex patterns and features of the data that cannot be described linearly.

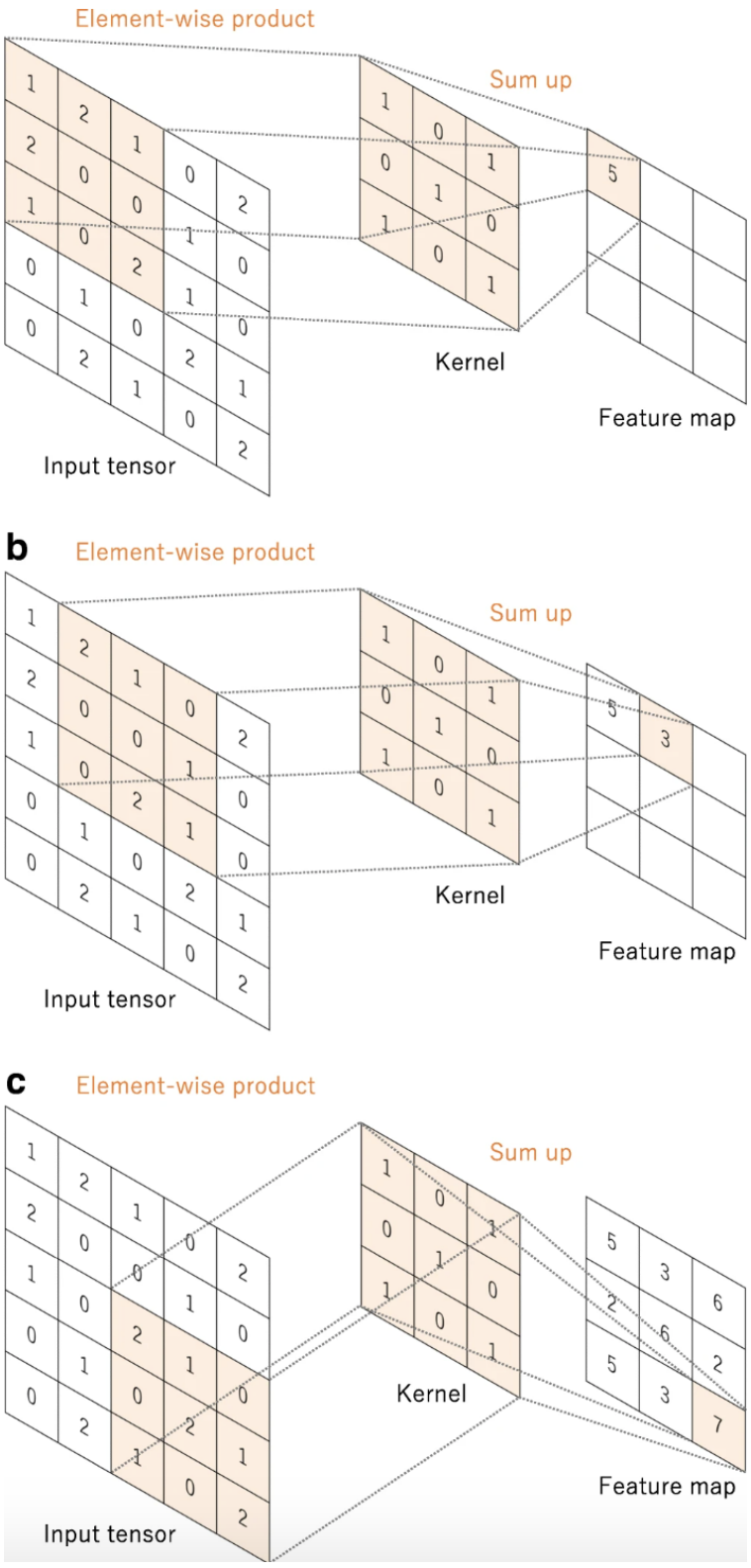

Figure 3.1: Depiction of the convolution of a two-dimensional input tensor, reproduced from Yamashita et al. (2018) [2]. At each section that the kernel slides over, the matrix sum of the section and kernel is mapped to a new, output tensor (labeled ”Feature map”).

3.2 Gaussian Interpolation of Light Curves

LSST light curves, as presented in Figure 2.3, are not in the two-dimensional form required for CNN input data. Our pipeline thus must include a pre-processing step, in which light curves are interpolated via Gaussian Process regression (GPR). We use a two-dimensional kernel that computes covariance over wave band and time (these are then the two dimensions of our NN input matrix). Our kernel is optimized via the Python-based package `george` [46].

3.3 Network Architecture

The architecture of our network contains 2 convolutional layers, which feature ReLU (Rectified Linear Units) activation functions. The initial layer encompasses 64 filters, followed by the second layer with 32 filters. A flattening layer transforms the preceding matrix into a vector passed on to a fully-connected dense layer. This layer employs a Sigmoid activation function for binary classification and is followed by a final 2-neuron dense layer. For optimization, the model is compiled with the Adam optimizer [47] and utilizes a Binary Cross-Entropy loss function. This type of function, typically used for binary classification problems, gives a continuous measure of accuracy which is favorable for gradient-descent optimization. We train the data on a set of $\sim 10^4$ simulated light curves. Efficiency results of this network are explored in Chapter 4.

3.4 Detection Network for Pan-STARRS Light Curves

Our eruption model has recently been used in a pre-SN analysis of SN 2023ixf, a recent Type II SN of a dusty RSG progenitor star in the Pinwheel Galaxy (M101), by Ransome et al. (2023) [48]. This study searched for a precursor eruption preceding the supernova in light curve data from the Pan-STARRS observatory [49]. Photoionization lines in flash spectroscopic measurements of the SN imply the presence of a compact CSM surrounding the progenitor generated by heightened mass loss; Jacobson-Galán et al. (2023) used spectral modelling to constrain this CSM to radius $r = (.5 - 1) \times 10^{15}$ cm [50].

Ransome et al. constructed a multi-layer perceptron network (MLP). MLPs are "feed-forward" neural networks, meaning information travels in the forward direction exclusively (CNNs are also feed-forward, however, RNNs are *not*, as information "loops" in order for the network to retain memory from previous inputs) [51]. These networks consist of an input layer, at least one hidden layer, and an output layer, and are powered largely by their non-linear activation functions.

The network was trained on light curves constructed in the depth and cadence of Pan-STARRS data with injections of our model. The distance and ejecta velocity were fixed at the distance of

M101 (6.9 Mpc) and the measured velocity obtained from flash-spectroscopic measurements by Zhang et al. (2023), which found $v_{ej} \sim 50$ km/s [52]. Burst luminosity, ejecta mass, and progenitor radius are then the remaining free parameters specific to the eruption.

The study found no detectable eruption present in the light curve data. The absence of detection allowed strong limits to be placed on the luminosity and ejecta mass of any eruption that did take place. By generating network efficiency curves over free parameters, Ransome et al. were able to constrain the burst luminosity to $L_0 < 5 \times 10^4 L_\odot$. An upper limit for the ejecta mass of $.3 M_\odot$ was also found, which is consistent with other estimates of CSM mass of $\sim 5 \times 10^{-5} M_\odot$ [53] and $.001 - .03 M_\odot$ [54].

Chapter 4

Network Capabilities and Discussion

We now evaluate the efficiency of our network in detecting precursors as a function of our free parameters. This efficiency data allows us to predict distances at which precursor detections are possible, and, subsequently detection rates. Moreover, this analysis provides insight into the populations of eruptions–in terms of where they fall in parameter space–that our network can reliably detect. Once the network is in use, understanding its performance capabilities over different population distributions opens the possibility of reversing the problem and determining parameter populations from empirical detection rates. Subsequent conclusions may be drawn regarding the underlying process driving pre-SN eruptions.

4.1 Parameter Space Efficiency

We begin by investigating how our network performs over the three free parameters specific to our model: ejecta mass, ejecta velocity, and burst luminosity. To do so, we calculate the CNN's completeness–i.e., the fraction of bursts that it successfully detects as a function of these parameters. In figure 4.1, we create two-dimensional plots of this metric over each combination of free parameters. These plots are effectively slices of the model's three-dimensional parameter space efficiency; in each one, one of the parameters is held constant. We generate these plots at three representative distances: 20 Mpc, 200 Mpc, and 250 Mpc. The network displays high efficiency at low redshifts. We see this rapidly drop off at higher distances across all parameters. See Section 4.2 (below) for further analysis of network efficiency over redshift.

The parameter-space efficiency reveals that our neural network is most sensitive to the injected burst luminosity. This is unsurprising, as the mass and velocity of the material ejected both have no effect on the peak magnitude of the burst. Due to the dim nature of these bursts, detection is primarily constrained by the magnitude limits of the LSST (the 5σ depth of a single-visit observation will be ~ 24.5 in the r band [38]). Efficiency begins to fall off at $L \sim 10^6 L_\odot$. At the lower end of the luminosity range, $L = 10^5 L_\odot$, the network's capacity for detections is virtually nonexistent.

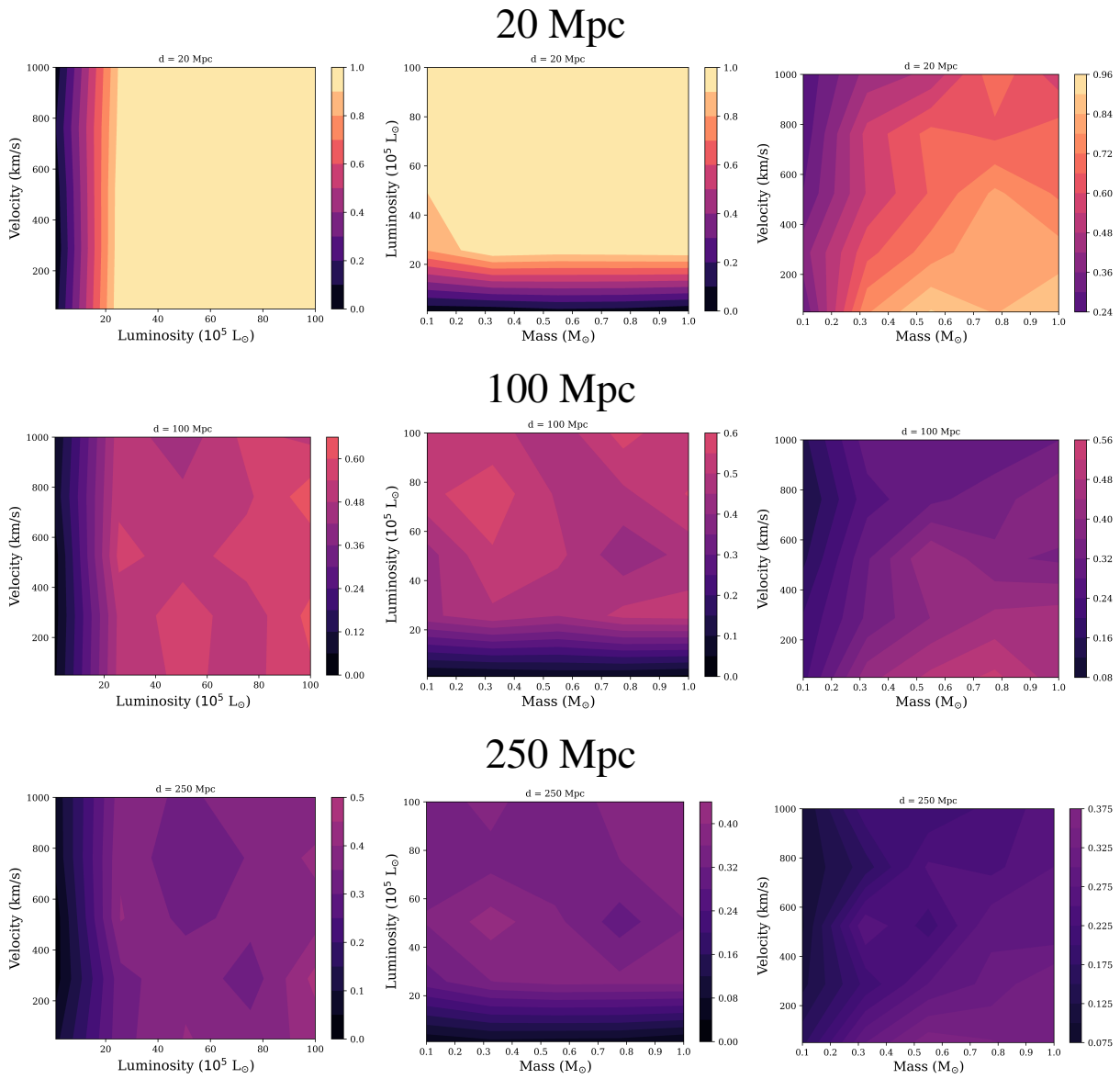

Figure 4.1: Network efficiency over the model free parameters L_0, v, and M. Efficiency is computed as completeness (the fraction of true bursts that the network accurately detects). Each plot displays the efficiency as a function of two parameters while the third is held constant. The constant parameter values are set to $M = 1M_\odot$, $v = 50$ km/s, and $L_0 = 10^6 L_\odot$. We present these plots for 3 representative distances: 20 Mpc (top row), 100 Mpc, (middle row), and 250 Mpc (bottom row).

4.2 Redshift Efficiency and Detection Rates

The overall completeness of our network as a function of redshift is calculated for different population distributions of the three remaining free parameters (ejecta mass, velocity, and burst luminosity). Specifically, we investigate the case in which these parameters fall on a uniform distribution and one in which they fall on log-uniform distributions, such that the lowest values of the assigned ranges (refer to Section 2.1 for ranges) are favored. The two populations that we compare represent "worst case" and "best case" scenarios, providing a benchmark for the network's capacity for detections. The log-uniform population consists of dimmer eruptions with faster fall times (refer to Figure 2.1), rendering eruptions more difficult to detect. We explore the potential populations of these parameters below in Section 4.3.

We plot the redshift efficiency curves in Figure 4.2. We find that our network, in general, can reliably make detections for redshifts $z \lesssim .03$. The uniform case displays much higher efficiency up until a drop off at $z \sim .015$. This reveals that even our most optical outcomes are strongly limited by distance. In the case of log-uniform parameter distributions, our network capabilities are even more limited, as our greatest efficiency at the closest distances is only $\sim 30\%$. Detections are then highly improbable for this population at $z \gtrsim .015$. Given the significant reliance of our network efficiency on luminosity, as depicted in Figure 4.1, this is to be expected. The main determinant of our detection rates will be the energy of these eruptions.

We then use these efficiency functions to calculate the number of detections we expect per year for type II SNe:

$$N = R_0 \int_{z_{min}}^{z_{max}} \frac{4\pi\epsilon(z)}{1+z} \frac{dV}{dz} dz$$

For this calculation, we use the volumetric rate, R_0, of SNe II at redshift z=0 (this approximation is sufficient given the small redshifts in consideration) obtained from Kessler et al. (2019) [55]. We assume that only one eruption precedes each supernova, but note that multiple eruptions corresponding to different stellar nuclear burning stages may be possible. For the log-uniform population that represents our lower detection limit, we estimate our network to be capable of successfully detecting precursors in $\sim$11 SN each year. Conversely, assuming uniform distributions of parameters, we expect a detection rate of $\sim$50 SN per year.

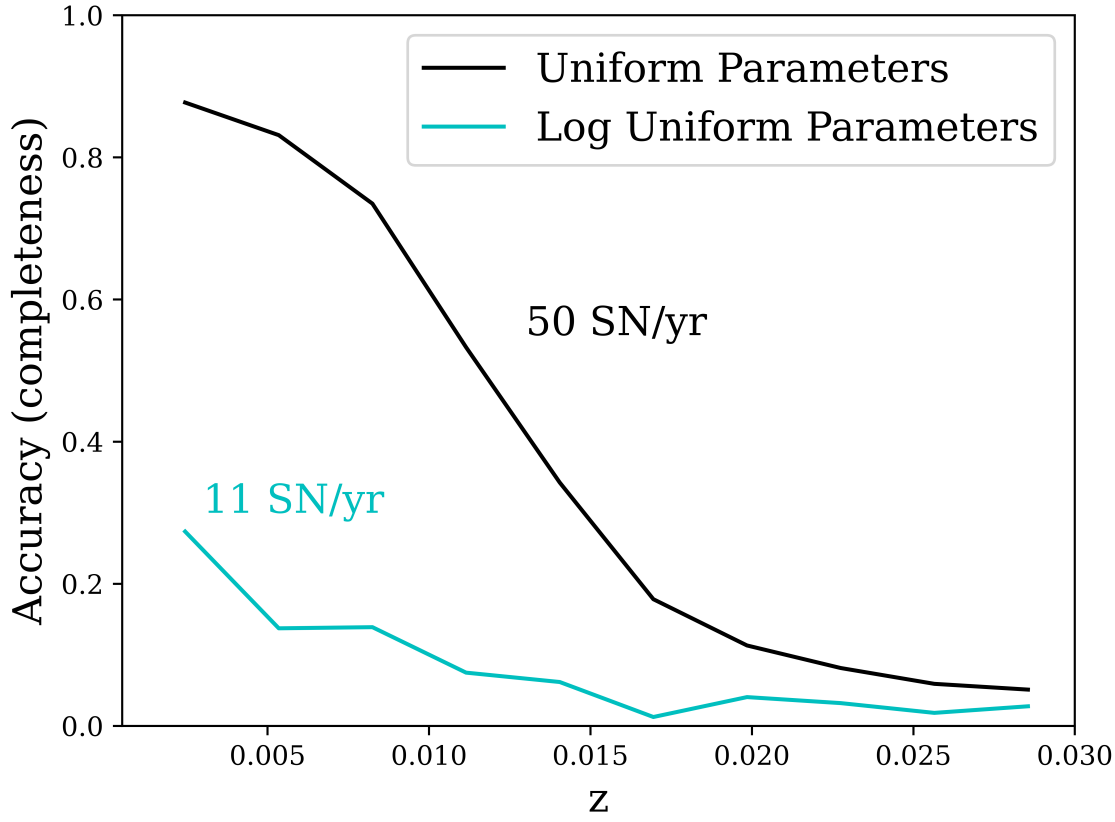

Figure 4.2: Network efficiency over redshift (z) corresponding to a uniform distribution of free parameters (black) and log-uniform distribution (blue). The corresponding detection rates for each case are provided.

4.3 Population Dependencies

The uncertainty in our anticipated detection rates reflects significant uncertainties regarding the very nature of these eruptions. Since we lack empirical observations, it is difficult to make assertions about how pre-SN bursts typically manifest. We look to radiation hydrodynamical models of wave-driven eruptions to gain better insight into where they might fall in our parameter space. Recent simulations conducted by Ko et al. (2022) [56] and Tsuna et al. (2023) [57] present six different burst models–three in which a single eruption occurs, and three in which two eruptions occur. Within these two cases, energy injected into the envelope is varied between values of .3 and .8 times the binding energy of the envelope, which is equal to 4.86×10^{47} erg for the $15 M_{\odot}$ model used. In general, the binding energy for RSGs is on the order of 10^{47} ergs). In the case of two eruptions, they also vary the time between energy injections.

For single eruption cases, Tsuna et al. find peak luminosities ranging within $1 - 3 \times 10^{39}$ erg/s. Double eruption light curves exhibit a slightly higher peak range: $4 - 6 \times 10^{39}$ erg/s. This

small range falls on the lower end of our luminosity range just under where network efficiency falls off. They additionally find that the duration of energy injection has little effect on resultant peak luminosities. Energy injection simulates the energy produced by the nuclear burning process that generates bursts; hence, this duration time represents the duration over which the process takes place and dissipates energy into the stellar envelope. We consider the case in which precursor populations adhere to this luminosity range (maintaining the lower limit log distributions for velocity and mass), and compute a successful detection rate of 15 SN/yr, which falls only slightly higher than our lower limit estimation.

The inferred masses of the dense CSM in spectroscopic SN measurements suggest that mass could fall closer to a uniform distribution [57]. Adjusting only the mass population to a uniform one in the previous calculation–in which luminosity is held on the order of 10^{39} erg/s–yields a detection rate slightly higher, at 20 SN/yr. Finally, Tsuna et al. find ejecta velocities in the outermost part of the photosphere ~ 100 km/s, however, velocities derived from spectral measurements of Hα in SNe IIn range from $100 - 1000$ km/s [57]. If we assume a uniform distribution of velocity as well as mass, this shifts our estimated detection rate to 25 SN/yr.

We note that even the absence of precursor detections in LSST data by our network can provide valuable insights into the nature of these events. Similar to the analysis of SN 2023ixf (Section 3.4), but on a much larger scale due to the sheer volume of SNe that LSST will detect, our network will be able to place substantial limits on potential precursor events that go undetected. This information can still significantly contribute to our understanding of precursor events and their associated mechanisms. If no detections are made over 10 years, this would imply significant shortcomings in the current theories and models of the nuclear burning eruption mechanism. It may indicate that an entirely different mechanism is responsible for late-stage mass loss, which manifests at much lower luminosities than those predicted by the wave-burning models.

Finally, more work may be done in exploring the parameter space of our model and how it affects network performance. Our study considers an ejecta mass range between .1 $M_\odot$ and 1 $M_\odot$. However, it should be noted that simulations such as in Tsuna et al. (2023) derive a range that extends much lower, down to $M_{ej} \sim .01 M_\odot$. Additionally, our models held progenitor radius R_0 at a fixed value of 1500 $R_\odot$. This represents an upper limit of RSG radii; the larger progenitor radius in our model results in slightly faster decay times of the burst luminosity. The dependence of our light curves on radius is provided in Figure 4.3. Changing this free parameter within our light curve sets may provide minimally different efficiency and rate results than what has been found thus far.

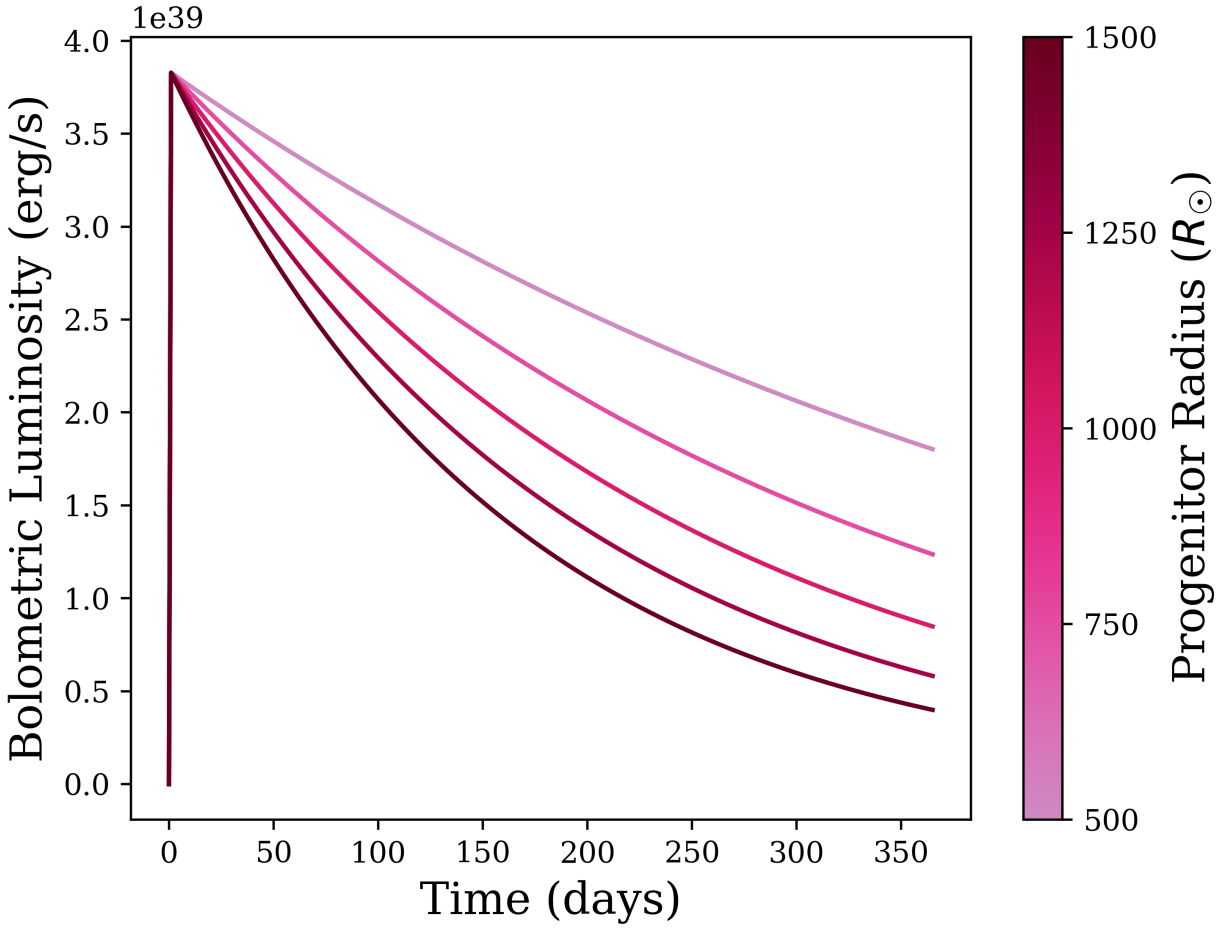

Figure 4.3: Bolometric light curves of the model eruption plotted over the range of progenitor radii R_0. Other free parameters are held constant at $L_0 = 10^6 L_\odot$, and $v = 50$ km/s, and $M = 1 M_\odot$.

Chapter 5

Conclusion

The variation and uncertainty in our predicted detection capabilities underscores the large uncertainty encompassing the problem at hand. We stress that the lack of observation and modeling capabilities renders these processes largely ambiguous, and thus difficult to predict. It is important to acknowledge the limitations in our approach; given the nuanced and diverse nature of precursor events, along with their faint signatures, our CNN will not capture every precursor event present in observational data. However, our efforts represent a significant step in the quest to observe and demystify them.

Despite potential limitations, the unconventional utilization of a CNN for analyzing multi-wavelength time series data in this study opens up new avenues for similar analysis problems, especially those that deal with large-scale surveys such as the LSST. The ability of CNNs to process vast amounts of data simultaneously and discern complex patterns within multi-dimensional datasets positions them as effective tools for other astrophysical problems. In general, our study underscores the essential role of neural networks in modern astrophysical research. Their adaptability and scalability make them invaluable for handling the abundance of data generated by contemporary observational facilities. By leveraging the capabilities of neural networks, astronomers can extract meaningful insights from vast datasets, leading to advancements in our understanding of the universe.

Our work lays a foundation for future research directions to deepen our understanding of RSGs and their role in stellar evolution. One promising avenue is extending our methodology to other modern transient surveys. The Zwicky Transient Facility (ZTF) [58], for example, is a northern sky survey based in the Palomar observatory that can also serve as a source for identifying precursors. By adapting and optimizing our techniques to the depth and cadence of this survey, we may be able to extend observational data even further and subsequently advance our understanding of RSG stellar evolution. Through continued interdisciplinary efforts, we can expect further progress in understanding the intricate processes that govern the life cycles of massive stars.

Bibliography

[1] Tatsuya Nakaoka, Koji S. Kawabata, Keiichi Maeda, Masaomi Tanaka, Masayuki Yamanaka, Takashi J. Moriya, Nozomu Tominaga, Tomoki Morokuma, Katsutoshi Takaki, Miho Kawabata, Naoki Kawahara, Ryosuke Itoh, Kensei Shiki, Hiroki Mori, Jun Hirochi, Taisei Abe, Makoto Uemura, Michitoshi Yoshida, Hiroshi Akitaya, Yuki Moritani, Issei Ueno, Takeshi Urano, Mizuki Isogai, Hidekazu Hanayama, and Takahiro Nagayama. The low-luminosity type iip supernova 2016bkv with early-phase circumstellar interaction. *The Astrophysical Journal*, 859:78, June 2018. ADS Bibcode: 2018ApJ...859...78N.

[2] Rikiya Yamashita, Mizuho Nishio, Richard Kinh Gian Do, and Kaori Togashi. Convolutional neural networks: an overview and application in radiology. *Insights into Imaging*, 9(44):611–629, August 2018.

[3] Stephen J. Smartt. Progenitors of core-collapse supernovae. *Annual Review of Astronomy and Astrophysics*, 47:63–106, September 2009.

[4] Gururaj A. Wagle, Alak Ray, Ajay Dev, and Adarsh Raghu. Type iip supernova progenitors and their explodability. i. convective overshoot, blue loops, and surface composition. *The Astrophysical Journal*, 886(1):27, November 2019.

[5] Nathan Smith. Mass loss: Its effect on the evolution and fate of high-mass stars. *Annual Review of Astronomy and Astrophysics*, 52:487–528, August 2014.

[6] Emily M. Levesque, Philip Massey, K. A. G. Olsen, and Bertrand Plez. Late-type red supergiants: Too cool for the magellanic clouds? *The Astrophysical Journal*, 667:202–212, September 2007. ADS Bibcode: 2007ApJ...667..202L.

[7] Emily M. Levesque. *Astrophysics of Red Supergiants*. IOP Publishing, December 2017.

[8] G. Meynet, V. Chomienne, S. Ekström, C. Georgy, A. Granada, J. Groh, A. Maeder, P. Eggenberger, E. Levesque, and P. Massey. Impact of mass-loss on the evolution and pre-supernova properties of red supergiants. *Astronomy and Astrophysics*, 575:A60, March 2015.

[9] Philip Massey, Bertrand Plez, Emily M. Levesque, K. A. G. Olsen, Geoffrey C. Clayton, and Eric Josselin. The Reddening of Red Supergiants: When Smoke Gets in Your Eyes. *The Astrophysical Journal*, 634(2):1286–1292, December 2005.

[10] W. C. Danchi, M. Bester, C. G. Degiacomi, L. J. Greenhill, and C. H. Townes. Characteristics of dust shells around 13 late-type stars. *Astronomical Journal*, 107:1469–1513, April 1994.

[11] Michael T. Schuster, Roberta M. Humphreys, and Massimo Marengo. The Circumstellar Environments of NML Cygni and the Cool Hypergiants. *Astronomical Journal*, 131(1):603–611, January 2006.

[12] Sung-Chul Yoon and Matteo Cantiello. Evolution of Massive Stars with Pulsation-driven Superwinds During the Red Supergiant Phase. *The Astrophysical Journall*, 717(1):L62–L65, July 2010.

[13] L. Hartmann and E. H. Avrett. On the extended chromosphere of alpha Orionis. *The Astrophysical Journal*, 284:238–249, September 1984.

[14] S. Ekström, C. Georgy, P. Eggenberger, G. Meynet, N. Mowlavi, A. Wyttenbach, A. Granada, T. Decressin, R. Hirschi, U. Frischknecht, C. Charbonnel, and A. Maeder. Grids of stellar models with rotation. i. models from 0.8 to 120 m at solar metallicity (z = 0.014). *Astronomy and Astrophysics*, 537:A146, January 2012. ADS Bibcode: 2012AA...537A.146E.

[15] Philip Massey, Kathryn F. Neugent, Sylvia Ekström, Cyril Georgy, and Georges Meynet. The time-averaged mass-loss rates of red supergiants as revealed by their luminosity functions in m31 and m33. *The Astrophysical Journal*, 942(2):69, January 2023.

[16] Emma R. Beasor, Ben Davies, Nathan Smith, Jacco Th van Loon, Robert D. Gehrz, and Donald F. Figer. A new mass-loss rate prescription for red supergiants. *Monthly Notices of the Royal Astronomical Society*, 492:5994–6006, March 2020. ADS Bibcode: 2020MNRAS.492.5994B.

[17] Viktoriya Morozova, Anthony L. Piro, Jim Fuller, and Schuyler D. van Dyk. The influence of late-stage nuclear burning on red supergiant supernova light curves. *The Astrophysical Journal Letters*, 891, 2020.

[18] F. Förster, T. J. Moriya, J. C. Maureira, J. P. Anderson, S. Blinnikov, F. Bufano, G. Cabrera-Vives, A. Clocchiatti, T. de Jaeger, P. A. Estévez, L. Galbany, S. González-Gaitán, G. Gräfener, M. Hamuy, E. Y. Hsiao, P. Huentelemu, P. Huijse, H. Kuncarayakti, J. Martínez, G. Medina, F. Olivares E., G. Pignata, A. Razza, I. Reyes, J. San Martín, R. C. Smith, E. Vera,

A. K. Vivas, A. de Ugarte Postigo, S.-C. Yoon, C. Ashall, M. Fraser, A. Gal-Yam, E. Kankare, L. Le Guillou, P. A. Mazzali, N. A. Walton, and D. R. Young. The delay of shock breakout due to circumstellar material evident in most type ii supernovae. *Nature Astronomy*, 2(1010):808–818, October 2018.

[19] WV Jacobson-Galán, Luc Dessart, DO Jones, Raffaella Margutti, DL Coppejans, Georgios Dimitriadis, Ryan J Foley, Charles D Kilpatrick, David J Matthews, Sofia Rest, et al. Final moments. i. precursor emission, envelope inflation, and enhanced mass loss preceding the luminous type ii supernova 2020tlf. *The Astrophysical Journal*, 924(1):15, 2022.

[20] D. Khazov, O. Yaron, A. Gal-Yam, I. Manulis, A. Rubin, S. R. Kulkarni, I. Arcavi, M. M. Kasliwal, E. O. Ofek, Y. Cao, D. Perley, J. Sollerman, A. Horesh, M. Sullivan, A. V. Filippenko, P. E. Nugent, D. A. Howell, S. B. Cenko, J. M. Silverman, H. Ebeling, F. Taddia, J. Johansson, R. R. Laher, J. Surace, U. D. Rebbapragada, P. R. Wozniak, and T. Matheson. Flash spectroscopy: Emission lines from the ionized circumstellar material around ¡10-day-old type ii supernovae. *The Astrophysical Journal*, 818:3, February 2016. ADS Bibcode: 2016ApJ...818....3K.

[21] O. Yaron, D. A. Perley, A. Gal-Yam, J. H. Groh, A. Horesh, E. O. Ofek, S. R. Kulkarni, J. Sollerman, C. Fransson, A. Rubin, P. Szabo, N. Sapir, F. Taddia, S. B. Cenko, S. Valenti, I. Arcavi, D. A. Howell, M. M. Kasliwal, P. M. Vreeswijk, D. Khazov, O. D. Fox, Y. Cao, O. Gnat, P. L. Kelly, P. E. Nugent, A. V. Filippenko, R. R. Laher, P. R. Wozniak, W. H. Lee, U. D. Rebbapragada, K. Maguire, M. Sullivan, and M. T. Soumagnac. Confined dense circumstellar material surrounding a regular type ii supernova. *Nature Physics*, 13:510–517, February 2017. ADS Bibcode: 2017NatPh..13..510Y.

[22] Rachel J. Bruch, Avishay Gal-Yam, Steve Schulze, Ofer Yaron, Yi Yang, Maayane Soumagnac, Mickael Rigault, Nora L. Strotjohann, Eran Ofek, Jesper Sollerman, Frank J. Masci, Cristina Barbarino, Anna Y. Q. Ho, Christoffer Fremling, Daniel Perley, Jakob Nordin, S. Bradley Cenko, S. Adams, Igor Adreoni, Eric C. Bellm, Nadia Blagorodnova, Mattia Bulla, Kevin Burdge, Kishalay De, Suhail Dhawan, Andrew J. Drake, Dmitry A. Duev, Alison Dugas, Matthew Graham, Melissa L. Graham, Ido Irani, Jacob Jencson, Emir Karamehmetoglu, Mansi Kasliwal, Young-Lo Kim, Shrinivas Kulkarni, Thomas Kupfer, Jingyi Liang, Ashish Mahabal, A. A. Miller, Thomas A. Prince, Reed Riddle, Y. Sharma, Roger Smith, Francesco Taddia, Kirsty Taggart, Richard Walters, and Lin Yan. A large fraction of hydrogen-rich supernova progenitors experience elevated mass loss shortly prior to explosion. *The Astrophysical Journal*, 912:46, May 2021. ADS Bibcode: 2021ApJ...912...46B.

[23] E. Quataert and J. Shiode. Wave-driven mass loss in the last year of stellar evolution: setting the stage for the most luminous core-collapse supernovae: Wave-driven mass loss. *Monthly Notices of the Royal Astronomical Society: Letters*, 423(1):L92–L96, Jun 2012.

[24] Joshua H. Shiode and Eliot Quataert. Setting the stage for circumslar interaction in core-collapse supernovae. ii. wave-driven mass loss in supernova progenitors. *The Astrophysical Journal*, 780(1):96, Dec 2013.

[25] Samantha Wu and Jim Fuller. A diversity of wave-driven presupernova outbursts. *The Astrophysical Journal*, 906:3, January 2021. ADS Bibcode: 2021ApJ...906....3W.

[26] Jim Fuller. Pre-supernova outbursts via wave heating in massive stars – i. red supergiants. *Monthly Notices of the Royal Astronomical Society*, 470(2):1642–1656, may 2017.

[27] Tatsuya Matsumoto and Brian D. Metzger. Supernova precursor emission and the origin of pre-explosion stellar mass-loss, 2022.

[28] Eran O. Ofek, Mark Sullivan, Nir J. Shaviv, Aviram Steinbok, Iair Arcavi, Avishay Gal-Yam, David Tal, Shrinivas R. Kulkarni, Peter E. Nugent, Sagi Ben-Ami, Mansi M. Kasliwal, S. Bradley Cenko, Russ Laher, Jason Surace, Joshua S. Bloom, Alexei V. Filippenko, Jeffrey M. Silverman, and Ofer Yaron. Precursors prior to type iin supernova explosions are common: Precursor rates, properties, and correlations. *The Astrophysical Journal*, 789:104, July 2014. ADS Bibcode: 2014ApJ...789..104O.

[29] Jon C. Mauerhan, Nathan Smith, Alexei Filippenko, Kyle Blanchard, Peter Blanchard, Chadwick F. E. Casper, S. Bradley Cenko, Kelsey I. Clubb, Daniel Cohen, Kiera Fuller, Gary Li, and Jeffrey M. Silverman. The unprecedented 2012 outburst of sn 2009ip: A luminous blue variable becomes a true supernova. *Monthly Notices of the Royal Astronomical Society*, 430(3):1801–1810, April 2013. arXiv:1209.6320 [astro-ph].

[30] Jon Mauerhan, G. Grant Williams, Nathan Smith, Paul S. Smith, Alexei V. Filippenko, Jennifer L. Hoffman, Peter Milne, Douglas C. Leonard, Kelsey I. Clubb, Ori D. Fox, and Patrick L. Kelly. Multi-epoch spectropolarimetry of SN 2009ip: direct evidence for aspherical circumstellar material. *Monthly Notices of the Royal Astronomical Society*, 442(2):1166–1180, jun 2014.

[31] E. O. Ofek, M. Sullivan, S. B. Cenko, M. M. Kasliwal, A. Gal-Yam, S. R. Kulkarni, I. Arcavi, L. Bildsten, J. S. Bloom, A. Horesh, D. A. Howell, A. V. Filippenko, R. Laher, D. Murray, E. Nakar, P. E. Nugent, J. M. Silverman, N. J. Shaviv, J. Surace, and O. Yaron. An outburst

from a massive star 40 days before a supernova explosion. *Nature*, 494:65–67, February 2013. ADS Bibcode: 2013Natur.494...65O.

[32] M. Fraser, M. Magee, R. Kotak, S. J. Smartt, K. W. Smith, J. Polshaw, A. J. Drake, T. Boles, C. H. Lee, W. S. Burgett, K. C. Chambers, P. W. Draper, H. Flewelling, K. W. Hodapp, N. Kaiser, R. P. Kudritzki, E. A. Magnier, P. A. Price, J. L. Tonry, R. J. Wainscoat, and C. Waters. Detection of an Outburst One Year Prior to the Explosion of SN 2011ht. *The Astrophysical Journal*, 779(1):L8, December 2013.

[33] A. Nyholm, J. Sollerman, F. Taddia, C. Fremling, T. J. Moriya, E. O. Ofek, A. Gal-Yam, A. De Cia, R. Roy, M. M. Kasliwal, Y. Cao, P. E. Nugent, and F. J. Masci. The bumpy light curve of type iin supernova iptf13z over 3 years. *Astronomy and Astrophysics*, 605:A6, August 2017.

[34] L. Tartaglia, A. Pastorello, M. Sullivan, C. Baltay, D. Rabinowitz, P. Nugent, A. J. Drake, S. G. Djorgovski, A. Gal-Yam, S. Fabrika, E. A. Barsukova, V. P. Goranskij, A. F. Valeev, T. Fatkhullin, S. Schulze, A. Mehner, F. E. Bauer, S. Taubenberger, J. Nordin, S. Valenti, D. A. Howell, S. Benetti, E. Cappellaro, G. Fasano, N. Elias-Rosa, M. Barbieri, D. Bettoni, A. Harutyunyan, T. Kangas, E. Kankare, J. C. Martin, S. Mattila, A. Morales-Garoffolo, P. Ochner, Umaa D. Rebbapragada, G. Terreran, L. Tomasella, M. Turatto, E. Verroi, and P. R. Woźniak. Interacting supernovae and supernova impostors. lsq13zm: an outburst heralds the death of a massive star. *Monthly Notices of the Royal Astronomical Society*, 459:1039–1059, June 2016. ADS Bibcode: 2016MNRAS.459.1039T.

[35] A. Pastorello, C. S. Kochanek, M. Fraser, Subo Dong, N. Elias-Rosa, A. V. Filippenko, S. Benetti, E. Cappellaro, L. Tomasella, A. J. Drake, J. Harmanen, T. Reynolds, B. J. Shappee, S. J. Smartt, K. C. Chambers, M. E. Huber, K. Smith, K. Z. Stanek, E. J. Christensen, L. Denneau, S. G. Djorgovski, H. Flewelling, C. Gall, A. Gal-Yam, S. Geier, A. Heinze, T. W. S. Holoien, J. Isern, T. Kangas, E. Kankare, R. A. Koff, J. M. Llapasset, T. B. Lowe, P. Lundqvist, E. A. Magnier, S. Mattila, A. Morales-Garoffolo, R. Mutel, J. Nicolas, P. Ochner, E. O. Ofek, E. Prosperi, A. Rest, Y. Sano, B. Stalder, M. D. Stritzinger, F. Taddia, G. Terreran, J. L. Tonry, R. J. Wainscoat, C. Waters, H. Weiland, M. Willman, D. R. Young, and W. Zheng. Supernovae 2016bdu and 2005gl, and their link with SN 2009ip-like transients: another piece of the puzzle. *Monthly Notices of the Royal Astronomical Society*, 474(1):197–218, February 2018.

[36] A. Pastorello, A. Reguitti, A. Morales-Garoffolo, Z. Cano, S. J. Prentice, D. Hiramatsu, J. Burke, E. Kankare, R. Kotak, T. Reynolds, S. J. Smartt, S. Bose, P. Chen, E. Congiu,

S. Dong, S. Geier, M. Gromadzki, E. Y. Hsiao, S. Kumar, P. Ochner, G. Pignata, L. Tomasella, L. Wang, I. Arcavi, C. Ashall, E. Callis, A. de Ugarte Postigo, M. Fraser, G. Hosseinzadeh, D. A. Howell, C. Inserra, D. A. Kann, E. Mason, P. A. Mazzali, C. McCully, Ó. Rodríguez, M. M. Phillips, K. W. Smith, L. Tartaglia, C. C. Thöne, T. Wevers, D. R. Young, M. L. Pumo, T. B. Lowe, E. A. Magnier, R. J. Wainscoat, C. Waters, and D. E. Wright. A luminous stellar outburst during a long-lasting eruptive phase first, and then SN IIn 2018cnf. *Astronomy and Astrophysics*, 628:A93, August 2019.

[37] LSST Science Collaboration, Paul A. Abell, Julius Allison, Scott F. Anderson, John R. Andrew, J. Roger P. Angel, Lee Armus, David Arnett, S. J. Asztalos, Tim S. Axelrod, Stephen Bailey, D. R. Ballantyne, Justin R. Bankert, Wayne A. Barkhouse, Jeffrey D. Barr, L. Felipe Barrientos, Aaron J. Barth, James G. Bartlett, Andrew C. Becker, Jacek Becla, Timothy C. Beers, Joseph P. Bernstein, Rahul Biswas, Michael R. Blanton, Joshua S. Bloom, John J. Bochanski, Pat Boeshaar, Kirk D. Borne, Marusa Bradac, W. N. Brandt, Carrie R. Bridge, Michael E. Brown, Robert J. Brunner, James S. Bullock, Adam J. Burgasser, James H. Burge, David L. Burke, Phillip A. Cargile, Srinivasan Chandrasekharan, George Chartas, Steven R. Chesley, You-Hua Chu, David Cinabro, Mark W. Claire, Charles F. Claver, Douglas Clowe, A. J. Connolly, Kem H. Cook, Jeff Cooke, Asantha Cooray, Kevin R. Covey, Christopher S. Culliton, Roelof de Jong, Willem H. de Vries, Victor P. Debattista, Francisco Delgado, Ian P. Dell'Antonio, Saurav Dhital, Rosanne Di Stefano, Mark Dickinson, Benjamin Dilday, S. G. Djorgovski, Gregory Dobler, Ciro Donalek, Gregory Dubois-Felsmann, Josef Durech, Ardis Eliasdottir, Michael Eracleous, Laurent Eyer, Emilio E. Falco, Xiaohui Fan, Christopher D. Fassnacht, Harry C. Ferguson, Yanga R. Fernandez, Brian D. Fields, Douglas Finkbeiner, Eduardo E. Figueroa, Derek B. Fox, Harold Francke, James S. Frank, Josh Frieman, Sebastien Fromenteau, Muhammad Furqan, Gaspar Galaz, A. Gal-Yam, Peter Garnavich, Eric Gawiser, John Geary, Perry Gee, Robert R. Gibson, Kirk Gilmore, Emily A. Grace, Richard F. Green, William J. Gressler, Carl J. Grillmair, Salman Habib, J. S. Haggerty, Mario Hamuy, Alan W. Harris, Suzanne L. Hawley, Alan F. Heavens, Leslie Hebb, Todd J. Henry, Edward Hileman, Eric J. Hilton, Keri Hoadley, J. B. Holberg, Matt J. Holman, Steve B. Howell, Leopoldo Infante, Zeljko Ivezic, Suzanne H. Jacoby, Bhuvnesh Jain, R, Jedicke, M. James Jee, J. Garrett Jernigan, Saurabh W. Jha, Kathryn V. Johnston, R. Lynne Jones, Mario Juric, Mikko Kaasalainen, Styliani, Kafka, Steven M. Kahn, Nathan A. Kaib, Jason Kalirai, Jeff Kantor, Mansi M. Kasliwal, Charles R. Keeton, Richard Kessler, Zoran Knezevic, Adam Kowalski, Victor L. Krabbendam, K. Simon Krughoff, Shrinivas Kulkarni, Stephen Kuhlman, Mark Lacy, Sebastien Lepine, Ming Liang, Amy Lien, Paulina Lira, Knox S. Long, Suzanne Lorenz, Jennifer M. Lotz, R. H. Lupton, Julie Lutz, Lucas M. Macri, Ashish A. Mahabal, Rachel Mandelbaum, Phil Marshall, Morgan May, Peregrine M. McGehee, Brian T.

Meadows, Alan Meert, Andrea Milani, Christopher J. Miller, Michelle Miller, David Mills, Dante Minniti, David Monet, Anjum S. Mukadam, Ehud Nakar, Douglas R. Neill, Jeffrey A. Newman, Sergei Nikolaev, Martin Nordby, Paul O'Connor, Masamune Oguri, John Oliver, Scot S. Olivier, Julia K. Olsen, Knut Olsen, Edward W. Olszewski, Hakeem Oluseyi, Nelson D. Padilla, Alex Parker, Joshua Pepper, John R. Peterson, Catherine Petry, Philip A. Pinto, James L. Pizagno, Bogdan Popescu, Andrej Prsa, Veljko Radcka, M. Jordan Raddick, Andrew Rasmussen, Arne Rau, Jeonghee Rho, James E. Rhoads, Gordon T. Richards, Stephen T. Ridgway, Brant E. Robertson, Rok Roskar, Abhijit Saha, Ata Sarajedini, Evan Scannapieco, Terry Schalk, Rafe Schindler, Samuel Schmidt, Sarah Schmidt, Donald P. Schneider, German Schumacher, Ryan Scranton, Jacques Sebag, Lynn G. Seppala, Ohad Shemmer, Joshua D. Simon, M. Sivertz, Howard A. Smith, J. Allyn Smith, Nathan Smith, Anna H. Spitz, Adam Stanford, Keivan G. Stassun, Jay Strader, Michael A. Strauss, Christopher W. Stubbs, Donald W. Sweeney, Alex Szalay, Paula Szkody, Masahiro Takada, Paul Thorman, David E. Trilling, Virginia Trimble, Anthony Tyson, Richard Van Berg, Daniel Vanden Berk, Jake VanderPlas, Licia Verde, Bojan Vrsnak, Lucianne M. Walkowicz, Benjamin D. Wandelt, Sheng Wang, Yun Wang, Michael Warner, Risa H. Wechsler, Andrew A. West, Oliver Wiecha, Benjamin F. Williams, Beth Willman, David Wittman, Sidney C. Wolff, W. Michael Wood-Vasey, Przemek Wozniak, Patrick Young, Andrew Zentner, and Hu Zhan. LSST Science Book, Version 2.0. *arXiv e-prints*, page arXiv:0912.0201, December 2009.

[38] Željko Ivezić et al. LSST: From Science Drivers to Reference Design and Anticipated Data Products. *The Astrophysical Journal*, 873(2):111, March 2019.

[39] Kelly M. Hambleton et al. Rubin observatory lsst transients and variable stars roadmap. *Publications of the Astronomical Society of the Pacific*, 135(1052):105002, November 2023.

[40] W. D. Arnett. Analytic solutions for light curves of supernovae of Type II. *The Astrophysical Journal*, 237:541–549, April 1980.

[41] V. Ashley Villar, Edo Berger, Brian D. Metzger, and James Guillochon. Theoretical models of optical transients. i. a broad exploration of the duration–luminosity phase space. *The Astrophysical Journal*, 849(1):70, nov 2017.

[42] W. D. Arnett. Type I supernovae. I - Analytic solutions for the early part of the light curve. *The Astrophysical Journal*, 253:785–797, February 1982.

[43] Francisco Delgado, Abhijit Saha, Srinivasan Chandrasekharan, Kem Cook, Catherine Petry, and Stephen Ridgway. The lsst operations simulator. In *Modeling, Systems Engineering, and Project Management for Astronomy VI*, volume 9150, page 422–445. SPIE, August 2014.

[44] Robin M. Schmidt. Recurrent neural networks (rnns): A gentle introduction and overview. *arXiv e-prints*, November 2019. ADS Bibcode: 2019arXiv191205911S.

[45] Yann LeCun, Yoshua Bengio, and Geoffrey Hinton. Deep learning. *Nature*, 521(7553):436–444, May 2015.

[46] Sivaram Ambikasaran, Daniel Foreman-Mackey, Leslie Greengard, David W. Hogg, and Michael O'Neil. Fast direct methods for gaussian processes. *IEEE Transactions on Pattern Analysis and Machine Intelligence*, 38:252, June 2015. ADS Bibcode: 2015ITPAM..38..252A.

[47] Diederik P. Kingma and Jimmy Ba. Adam: A method for stochastic optimization, 2017.

[48] Conor L. Ransome, V. Ashley Villar, Anna Tartaglia, Sebastian Javier Gonzalez, Wynn V. Jacobson-Galán, Charles D. Kilpatrick, Raffaella Margutti, Ryan J. Foley, Matthew Grayling, Yuan Qi Ni, Ricardo Yarza, Christine Ye, Katie Auchettl, Thomas de Boer, Kenneth C. Chambers, David A. Coulter, Maria R. Drout, Diego Farias, Christa Gall, Hua Gao, Mark E. Huber, Adaeze L. Ibik, David O. Jones, Nandita Khetan, Chien-Cheng Lin, Collin A. Politsch, Sandra I. Raimundo, Armin Rest, Richard J. Wainscoat, S. Karthik Yadavalli, and Yossef Zenati. SN2023ixf in Messier 101: the twilight years of the progenitor as seen by Pan-STARRS. *arXiv e-prints*, page arXiv:2312.04426, December 2023.

[49] K. C. Chambers, E. A. Magnier, N. Metcalfe, H. A. Flewelling, M. E. Huber, C. Z. Waters, L. Denneau, P. W. Draper, D. Farrow, D. P. Finkbeiner, C. Holmberg, J. Koppenhoefer, P. A. Price, A. Rest, R. P. Saglia, E. F. Schlafly, S. J. Smartt, W. Sweeney, R. J. Wainscoat, W. S. Burgett, S. Chastel, T. Grav, J. N. Heasley, K. W. Hodapp, R. Jedicke, N. Kaiser, R. P. Kudritzki, G. A. Luppino, R. H. Lupton, D. G. Monet, J. S. Morgan, P. M. Onaka, B. Shiao, C. W. Stubbs, J. L. Tonry, R. White, E. Bañados, E. F. Bell, R. Bender, E. J. Bernard, M. Boegner, F. Boffi, M. T. Botticella, A. Calamida, S. Casertano, W. P. Chen, X. Chen, S. Cole, N. Deacon, C. Frenk, A. Fitzsimmons, S. Gezari, V. Gibbs, C. Goessl, T. Goggia, R. Gourgue, B. Goldman, P. Grant, E. K. Grebel, N. C. Hambly, G. Hasinger, A. F. Heavens, T. M. Heckman, R. Henderson, T. Henning, M. Holman, U. Hopp, W. H. Ip, S. Isani, M. Jackson, C. D. Keyes, A. M. Koekemoer, R. Kotak, D. Le, D. Liska, K. S. Long, J. R. Lucey, M. Liu, N. F. Martin, G. Masci, B. McLean, E. Mindel, P. Misra, E. Morganson, D. N. A. Murphy, A. Obaika, G. Narayan, M. A. Nieto-Santisteban, P. Norberg, J. A. Peacock, E. A. Pier, M. Postman, N. Primak, C. Rae, A. Rai, A. Riess, A. Riffeser, H. W. Rix, S. Röser, R. Russel, L. Rutz, E. Schilbach, A. S. B. Schultz, D. Scolnic, L. Strolger, A. Szalay, S. Seitz, E. Small, K. W. Smith, D. R. Soderblom, P. Taylor, R. Thomson, A. N. Taylor, A. R.

Thakar, J. Thiel, D. Thilker, D. Unger, Y. Urata, J. Valenti, J. Wagner, T. Walder, F. Walter, S. P. Watters, S. Werner, W. M. Wood-Vasey, and R. Wyse. The pan-starrs1 surveys, 2019.

[50] W. V. Jacobson-Galán, L. Dessart, R. Margutti, R. Chornock, R. J. Foley, C. D. Kilpatrick, D. O. Jones, K. Taggart, C. R. Angus, S. Bhattacharjee, L. A. Braff, D. Brethauer, A. J. Burgasser, F. Cao, C. M. Carlile, K. C. Chambers, D. A. Coulter, E. Dominguez-Ruiz, C. B. Dickinson, T. de Boer, A. Gagliano, C. Gall, H. Gao, E. L. Gates, S. Gomez, M. Guolo, M. R. J. Halford, J. Hjorth, M. E. Huber, M. N. Johnson, P. R. Karpoor, T. Laskar, N. LeBaron, Z. Li, Y. Lin, S. D. Loch, P. D. Lynam, E. A. Magnier, P. Maloney, D. J. Matthews, M. McDonald, H.-Y. Miao, D. Milisavljevic, Y.-C. Pan, S. Pradyumna, C. L. Ransome, J. M. Rees, A. Rest, C. Rojas-Bravo, N. R. Sandford, L. Sandoval Ascencio, S. Sanjaripour, A. Savino, H. Sears, N. Sharei, S. J. Smartt, E. R. Softich, C. A. Theissen, S. Tinyanont, H. Tohfa, V. A. Villar, Q. Wang, R. J. Wainscoat, A. L. Westerling, E. Wiston, M. A. Wozniak, S. K. Yadavalli, and Y. Zenati. Sn 2023ixf in messier 101: Photo-ionization of dense, close-in circumstellar material in a nearby type ii supernova. *The Astrophysical Journal Letters*, 954(2):L42, September 2023.

[51] Simon Haykin. *Neural Networks: A Comprehensive Foundation*. Prentice Hall, 1999.

[52] Jujia Zhang, Han Lin, Xiaofeng Wang, Zeyi Zhao, Liping Li, Jialian Liu, Shengyu Yan, Danfeng Xiang, Huijuan Wang, and Jinming Bai. Circumstellar material ejected violently by a massive star immediately before its death. *Science Bulletin*, 68(21):2548–2554, 2023.

[53] Charles D. Kilpatrick, Ryan J. Foley, Wynn V. Jacobson-Galán, Anthony L. Piro, Stephen J. Smartt, Maria R. Drout, Alexander Gagliano, Christa Gall, Jens Hjorth, David O. Jones, Kaisey S. Mandel, Raffaella Margutti, Enrico Ramirez-Ruiz, Conor L. Ransome, V. Ashley Villar, David A. Coulter, Hua Gao, David Jacob Matthews, Kirsty Taggart, and Yossef Zenati. Sn 2023ixf in messier 101: A variable red supergiant as the progenitor candidate to a type ii supernova. *The Astrophysical Journal Letters*, 952(1):L23, July 2023.

[54] Rishabh Singh Teja, Avinash Singh, Judhajeet Basu, G. C. Anupama, D. K. Sahu, Anirban Dutta, Vishwajeet Swain, Tatsuya Nakaoka, Utkarsh Pathak, Varun Bhalerao, Sudhanshu Barway, Harsh Kumar, Nayana A. J., Ryo Imazawa, Brajesh Kumar, and Koji S. Kawabata. Far-ultraviolet to near-infrared observations of sn 2023ixf: A high-energy explosion engulfed in complex circumstellar material. *The Astrophysical Journal Letters*, 954(1):L12, August 2023.

[55] R. Kessler, G. Narayan, A. Avelino, E. Bachelet, R. Biswas, P. J. Brown, D. F. Chernoff, A. J. Connolly, M. Dai, S. Daniel, R. Di Stefano, M. R. Drout, L. Galbany, S. González-Gaitán,

M. L. Graham, R. Hložek, E. E. O. Ishida, J. Guillochon, S. W. Jha, D. O. Jones, K. S. Mandel, D. Muthukrishna, A. O'Grady, C. M. Peters, J. R. Pierel, K. A. Ponder, A. Prša, S. Rodney, V. A. Villar, The LSST Dark Energy Science Collaboration, the Transient, and Variable Stars Science Collaboration. Models and simulations for the photometric lsst astronomical time series classification challenge (plasticc). *Publications of the Astronomical Society of the Pacific*, 131(1003):094501, September 2019.

[56] Takatoshi Ko, Daichi Tsuna, Yuki Takei, and Toshikazu Shigeyama. Eruption of the envelope of massive stars by energy injection with finite duration. *The Astrophysical Journal*, 930(2):168, May 2022. arXiv:2112.14909 [astro-ph].

[57] Daichi Tsuna, Yuki Takei, and Toshikazu Shigeyama. Precursors of supernovae from mass eruption: Prospects for early warning of nearby core-collapse supernovae. *The Astrophysical Journal*, 945(2):104, March 2023.

[58] Eric C. Bellm, Shrinivas R. Kulkarni, Matthew J. Graham, Richard Dekany, Roger M. Smith, Reed Riddle, Frank J. Masci, George Helou, Thomas A. Prince, Scott M. Adams, C. Barbarino, Tom Barlow, James Bauer, Ron Beck, Justin Belicki, Rahul Biswas, Nadejda Blagorodnova, Dennis Bodewits, Bryce Bolin, Valery Brinnel, Tim Brooke, Brian Bue, Mattia Bulla, Rick Burruss, S. Bradley Cenko, Chan-Kao Chang, Andrew Connolly, Michael Coughlin, John Cromer, Virginia Cunningham, Kishalay De, Alex Delacroix, Vandana Desai, Dmitry A. Duev, Gwendolyn Eadie, Tony L. Farnham, Michael Feeney, Ulrich Feindt, David Flynn, Anna Franckowiak, S. Frederick, C. Fremling, Avishay Gal-Yam, Suvi Gezari, Matteo Giomi, Daniel A. Goldstein, V. Zach Golkhou, Ariel Goobar, Steven Groom, Eugean Hacopians, David Hale, John Henning, Anna Y. Q. Ho, David Hover, Justin Howell, Tiara Hung, Daniela Huppenkothen, David Imel, Wing-Huen Ip, Željko Ivezić, Edward Jackson, Lynne Jones, Mario Juric, Mansi M. Kasliwal, S. Kaspi, Stephen Kaye, Michael S. P. Kelley, Marek Kowalski, Emily Kramer, Thomas Kupfer, Walter Landry, Russ R. Laher, Chien-De Lee, Hsing Wen Lin, Zhong-Yi Lin, Ragnhild Lunnan, Matteo Giomi, Ashish Mahabal, Peter Mao, Adam A. Miller, Serge Monkewitz, Patrick Murphy, Chow-Choong Ngeow, Jakob Nordin, Peter Nugent, Eran Ofek, Maria T. Patterson, Bryan Penprase, Michael Porter, Ludwig Rauch, Umaa Rebbapragada, Dan Reiley, Mickael Rigault, Hector Rodriguez, Jan van Roestel, Ben Rusholme, Jakob van Santen, S. Schulze, David L. Shupe, Leo P. Singer, Maayane T. Soumagnac, Robert Stein, Jason Surace, Jesper Sollerman, Paula Szkody, F. Taddia, Scott Terek, Angela Van Sistine, Sjoert van Velzen, W. Thomas Vestrand, Richard Walters, Charlotte Ward, Quan-Zhi Ye, Po-Chieh Yu, Lin Yan, and Jeffry Zolkower. The Zwicky Transient Facility: System Overview, Performance, and First Results. *Publications of the Astronomical Society of the Pacific*, 131(995):018002, January 2019.